ARTICLE

Reduction of MOC discretization errors through a minimization of source ratio variances

Masato Tabuchi[a,b*], Akio Yamamoto[a], Tomohiro Endo[a] and Masahiro Tatsumi[b]

[a] *Department of Material Physics and Energy Engineering, Graduate School of Engineering Nagoya University Furo-cho, Chikusa-ku, Nagoya 464-8603, Japan;* [b] *Nuclear Engineering Ltd., 1-3-7, Tosabori, Nishi-ku, Osaka 550-0001, Japan*

A new technique to reduce discretization errors for ray tracing in the method of characteristics (MOC) is proposed focusing on depletion calculations of single and multi assembly geometries. In order to efficiently carry out depletion calculations, a calculation scheme using the SPH method can be used. However, the discretization errors are caused by changes of neutron sources and total cross sections according to a depletion. This fact means that improvement of accuracy cannot be expected by the calculation scheme with the SPH method when changes of the above parameters are significant. In order to mitigate this problem, a new approach is developed. In the new approach, the discretization errors are reduced by minimizing a variance of a certain parameter which is composed of a ratio of neutron source to total cross section. The verification results suggest that accuracy is degraded by the SPH method as expected especially in a geometry where neutron sources and total cross sections are drastically changing through a depletion. On the other hand, the new approach gives more accurate results compared to the conventional MOC in all calculation cases. Consequently, improvement of calculation efficiency by the new approach is confirmed.

Keywords; reactor physics; method of characteristics; numerical analysis; discretization

[*]Corresponding author. Email: mtabuchi@neltd.co.jp

error; depletion calculation

1. Introduction

In the method of characteristics (MOC) [1], ray tracing parameters, which represent azimuthal angle division, polar angle division and ray separation, are important from the viewpoints of computational burden and accuracy. Although faster calculation can be carried out with coarser ray tracing parameters, accuracy would be degraded due to discretization errors. In order to reduce the discretization errors, several techniques have been proposed in the previous studies [2]-[6]. These techniques focus on a certain type of ray tracing parameter, i.e. polar angle division or ray separation. As an alternate approach, in the other previous study, the superhomogenization (SPH) method [7] is used to reduce all types of the discretization errors for ray tracing [8].

In this paper, a calculation scheme using the SPH method is considered as the first step of the present study. The SPH method is a kind of equivalence methods, by which a reference result can be reproduced with a coarse calculation condition, and is used to improve calculation efficiency in the previous studies [8]-[10]. Although the SPH method is originally a technique for reducing spatial homogenization errors, the SPH method can be used also for reducing discretization errors due to coarse ray tracing condition as described above. In general, the calculation procedure of the SPH method is as follows:

Step 1: Calculation with a fine condition is carried out to obtain a reference result.

Step 2: Calculation with a coarse condition using the SPH corrected cross sections (as shown in Equation (1)) is carried out:

$$\Sigma_{x,g,i}^{SPH} = \mu_{g,i}\Sigma_{x,g,i}\,, \tag{1}$$

where

$\Sigma_{x,g,i}$: cross section of reaction *x*, *g*-th energy group and *i*-th region,

$\mu_{g,i}$: the SPH factor of *g*-th energy group and *i*-th region.

Step 3: The SPH factors are evaluated by Equation (2):

$$\mu_{g,i} = \frac{\phi_{g,i}^{fine}}{\phi_{g,i}^{coarse}}, \tag{2}$$

where

$\phi_{g,i}^{coarse}$: neutron flux of *g*-th energy group and *i*-th region with a coarse condition,

$\phi_{g,i}^{fine}$: neutron flux of *g*-th energy group and *i*-th region with a fine condition.

Step 4: Steps 2 and 3 are iterated until the SPH factors get convergent.

Calculations in Steps 1 and 2 of this procedure have to be performed by eigenvalue calculations to completely reproduce a reference results. In order to reduce the additional calculation time for these steps, in the present study, fixed source calculations are performed instead of eigenvalue calculations.

As shown in the above procedures, additional calculations are necessary for the evaluation of the SPH factors. Especially, Step 1 would need huge computational time since calculation with a fine condition is performed. When the SPH factors are evaluated at all burnup steps, merit of the SPH method is cancelled out due to the additional calculations. Therefore, the SPH factors have to be evaluated only at a few burnup steps to improve calculation efficiency. The concept of the SPH method considered in the present study is illustrated in **Figure 1**. In the calculation procedure of Figure 1, the SPH factors are not prepared before a depletion calculation is begun. Therefore, additional calculations to evaluate the SPH factors are performed only at the first burnup step and at some burnup steps in which the discretization errors are predicted to be large.

< Figure 1 >

If the discretization errors are reduced by this approach, calculation efficiency is

expected to be improved, because accurate results can be obtained without significant additional computational time for the application of the SPH method. As the first step of the present study, the applicability of the SPH method to depletion calculations based on the above procedure is investigated. Then, as the next step, a new technique which is more suitable for depletion calculations is proposed by using a similar procedure with Figure 1. The purpose of the present study is to improve calculation efficiency of lattice calculations involving single and multi assemblies.

In section 2, equations for the discretization errors in the conventional MOC and the SPH method are derived to analyze causes of the errors. By using ideas in these derivations, a new approach is proposed to reduce the discretization errors. The derivation of the new approach is also shown in section 2. Some verifications through single and multi assembly calculations are carried out in section 3. Finally the conclusion of the present paper is summarized in section 4.

2. Derivation of equations for the discretization errors

2.1. Discretization errors in the conventional MOC

In this section, the equation for the discretization errors in the conventional MOC is derived to grasp how the discretization errors are caused. When the isotropic scattering is assumed and a discretization error of polar angle is eliminated, MOC is equivalent to the collision probability method. Although collision probabilities are not explicitly treated in ordinary MOC calculations, neutron balance equations using collision probabilities can be written as follows:

$$\Sigma_{t,g,j}^{(n)} \phi_{g,j}^{coarse(n)} V_j = \sum_i P_{g,ij}^{coarse(n)} Q_{g,i}^{(n)} V_i \,, \tag{3}$$

$$\Sigma_{t,g,j}^{(n)} \phi_{g,j}^{fine(n)} V_j = \sum_i P_{g,ij}^{fine(n)} Q_{g,i}^{(n)} V_i \,, \tag{4}$$

where

$\Sigma_{t,g,j}^{(n)}$: total cross section of *n*-th burnup step, *g*-th energy group and *j*-th region,

V_j : region volume of *j*-th region,

$Q_{g,i}^{(n)}$: neutron source of *n*-th burnup step, *g*-th energy group and *i*-th region,

$\phi_{g,j}^{coarse(n)}$: neutron flux of *n*-th burnup step, *g*-th energy group and *j*-th region with a coarse condition,

$\phi_{g,j}^{fine(n)}$: neutron flux of *n*-th burnup step, *g*-th energy group and *j*-th region with a fine condition,

$P_{g,ij}^{coarse(n)}$: collision probability of *n*-th burnup step, *g*-th energy group from *i*-th region to *j*-th region calculated with a coarse condition,

$P_{g,ij}^{fine(n)}$: collision probability of *n*-th burnup step, *g*-th energy group from *i*-th region to *j*-th region calculated with a fine condition.

It should be noted that neutron sources and cross sections obtained with a coarse condition are actually different from those obtained with a fine condition due to the discretization errors in the previous burnup steps (propagation of the discretization errors during burnup). However, in this study, those differences are ignored for simplicity. In other words, the discretization errors are assumed to be directly caused in collision probabilities, and as a result of a transport sweep, those errors have effects only on neutron fluxes. From Equations (3) and (4), the discretization errors of neutron fluxes can be written as the following equation:

$$\phi_{g,j}^{coarse(n)} - \phi_{g,j}^{fine(n)} = \frac{1}{\Sigma_{t,g,j}^{(n)} V_j} \sum_i \left(P_{g,ij}^{coarse(n)} - P_{g,ij}^{fine(n)} \right) Q_{g,i}^{(n)} V_i \,. \tag{5}$$

2.2.Discretization errors in the SPH method

The calculation procedure of the SPH method is described in section 1. As mentioned

in Section1, fixed source calculations are performed in Steps 1 and 2 of this procedure instead of eigenvalue calculations to reduce the additional calculation time for these steps. The neutron sources for the fixed source calculations are evaluated by one transport sweep with a coarse condition. If the transport sweep for the evaluation of neutron sources is iterated twice or more, better neutron sources would be obtained. However, we confirmed that one transport sweep with acceleration such as GCMR [11][12] gives appropriate neutron sources especially in single assembly calculations. It should be noted that this calculation scheme would not completely reproduce a reference result especially in large geometries because neutron sources used for the calculations of the SPH factors are not completely convergent and are not evaluated with a fine condition.

The equation for the discretization errors in the SPH method is discussed through the similar derivation in the previous sub-section. When the SPH factors are evaluated at *m*-th burnup step, the neutron balance equation at *n*-th burnup step can be written as Equation (6):

$$\mu_{g,j}^{[m]}\Sigma_{t,g,j}^{(n)}\phi_{g,j}^{SPH[m],(n)}V_j = \sum_i P_{g,ij}^{SPH[m](n)}Q_{g,i}^{(n)}V_i \,, \tag{6}$$

where

$\mu_{g,j}^{[m]}$: the SPH factor of *g*-th energy group and *j*-th region evaluated at *m*-th burnup step,

$\phi_{g,j}^{SPH[m],(n)}$: neutron flux of *n*-th burnup step, *g*-th energy group and *j*-th region with the SPH factors evaluated at *m*-th burnup step,

$P_{g,ij}^{SPH[m],(n)}$: collision probability of *n*-th burnup step, *g*-th energy group from *i*-th region to *j*-th region with the SPH factors evaluated at *m*-th burnup step.

From Equations (4) and (6), the discretization errors of neutron fluxes for the SPH method can be written as the following equation:

$$\mu_{g,j}^{[m]}\phi_{g,j}^{SPH[m],(n)} - \phi_{g,j}^{fine(n)} = \frac{1}{\Sigma_{t,g,j}^{(n)}V_j}\sum_i \left(P_{g,ij}^{SPH[m],(n)} - P_{g,ij}^{fine(n)}\right)Q_{g,i}^{(n)}V_i \,. \tag{7}$$

In order to analyze the meaning of Equation (7), the right hand side of Equation (7) is separated into three parts as shown in Equation (8):

$$\begin{aligned}\mu_{g,j}^{[m]}\phi_{g,j}^{SPH[m],(n)}-\phi_{g,j}^{fine(n)} &= \frac{1}{\Sigma_{t,g,j}^{(n)}V_j}\sum_i\left(P_{g,ij}^{SPH[m],(m)}-P_{g,ij}^{fine(m)}\right)Q_{g,i}^{(m)}V_i \\ &+\frac{1}{\Sigma_{t,g,j}^{(n)}V_j}\sum_i\left(P_{g,ij}^{SPH[m],(n)}-P_{g,ij}^{fine(n)}\right)\left(Q_{g,i}^{(n)}-Q_{g,i}^{(m)}\right)V_i \\ &+\frac{1}{\Sigma_{t,g,j}^{(n)}V_j}\sum_i\left\{\left(P_{g,ij}^{SPH[m],(n)}-P_{g,ij}^{fine(n)}\right)-\left(P_{g,ij}^{SPH[m],(m)}-P_{g,ij}^{fine(m)}\right)\right\}Q_{g,i}^{(m)}V_i\end{aligned} \quad .(8)$$

From the reproducibility of the SPH method, reaction rates at *m*-th burnup step obtained by the SPH method become equivalent to those obtained with a fine condition. Therefore, Equation (9), which describes the equivalence of reaction rates, is satisfied:

$$\sum_i P_{g,ij}^{SPH[m],(m)}Q_{g,i}^{(m)}V_i=\sum_i P_{g,ij}^{fine(m)}Q_{g,i}^{(m)}V_i\,. \quad (9)$$

By using Equation (9), the first term of the right hand side of Equation (8) can be eliminated and Equation (8) can be transformed into the following equation:

$$\begin{aligned}\mu_{g,j}^{[m]}\phi_{g,j}^{SPH[m],(n)}-\phi_{g,j}^{fine(n)} &= \frac{1}{\Sigma_{t,g,j}^{(n)}V_j}\sum_i\left(P_{g,ij}^{SPH[m],(n)}-P_{g,ij}^{fine(n)}\right)\left(Q_{g,i}^{(n)}-Q_{g,i}^{(m)}\right)V_i \\ &+\frac{1}{\Sigma_{t,g,j}^{(n)}V_j}\sum_i\left\{\left(P_{g,ij}^{SPH[m],(n)}-P_{g,ij}^{fine(n)}\right)-\left(P_{g,ij}^{SPH[m],(m)}-P_{g,ij}^{fine(m)}\right)\right\}Q_{g,i}^{(m)}V_i\end{aligned} \quad . (10)$$

By using the following definitions shown in Equations (11) and (12), Equation (10) can be rewritten as Equation (13):

$$\Delta Q_{g,i}^{(m,n)}\equiv Q_{g,i}^{(n)}-Q_{g,i}^{(m)}\,, \quad (11)$$

$$\Delta P_{g,ij}^{(m,n)}\equiv P_{g,ij}^{(n)}-P_{g,ij}^{(m)}\,, \quad (12)$$

$$\mu_{g,j}^{[m]}\phi_{g,j}^{SPH[m],(n)} - \phi_{g,j}^{fine(n)} = \frac{1}{\Sigma_{t,g,j}^{(n)} V_j}\sum_i \left(P_{g,ij}^{SPH[m],(n)} - P_{g,ij}^{fine(n)}\right)\Delta Q_{g,i}^{(m,n)} V_i + \frac{1}{\Sigma_{t,g,j}^{(n)} V_j}\sum_i \left(\Delta P_{g,ij}^{SPH[m],(m,n)} - \Delta P_{g,ij}^{fine(m,n)}\right) Q_{g,i}^{(m)} V_i \quad . \tag{13}$$

The first term of the right hand side of Equation (13) depends on changes of neutron sources. And the second term of the right hand side comes from changes of total cross sections since changes of collision probabilities through a depletion is caused by only changes of total cross sections. Therefore, Equation (13) indicates that the discretization errors in the SPH method is caused by the changes of neutron sources and total cross sections. From this reason, in the SPH method, calculation accuracy would be degraded when neutron sources and total cross sections are drastically changing during a depletion calculation. Furthermore, a criterion for an update of the SPH factors is difficult to determine, since the changes of two parameters have effects on the discretization errors.

2.3.Derivation of a new approach and its discretization errors

As described in the previous sub-section, changes of neutron sources and total cross sections have effects on the discretization errors in the SPH method. In this section, a different approach, which can reduce the discretization errors due to changes of neutron sources, is proposed.

As the first step of the derivation, Equation (5), which describes the discretization error in the conventional MOC, is transformed into Equation (14) through the similar derivation in the previous sub-section:

$$\phi_{g,j}^{coarse(n)} - \phi_{g,j}^{fine(n)} = \frac{1}{\Sigma_{t,g,j}^{(n)} V_j} \sum_i \left(P_{g,ij}^{coarse(m)} - P_{g,ij}^{fine(m)} \right) Q_{g,i}^{(m)} V_i$$
$$+ \frac{1}{\Sigma_{t,g,j}^{(n)} V_j} \sum_i \left(P_{g,ij}^{coarse(n)} - P_{g,ij}^{fine(n)} \right) \left(Q_{g,i}^{(n)} - Q_{g,i}^{(m)} \right) V_i \quad . \quad (14)$$
$$+ \frac{1}{\Sigma_{t,g,j}^{(n)} V_j} \sum_i \left\{ \left(P_{g,ij}^{coarse(n)} - P_{g,ij}^{fine(n)} \right) - \left(P_{g,ij}^{coarse(m)} - P_{g,ij}^{fine(m)} \right) \right\} Q_{g,i}^{(m)} V_i$$

Equation (14) can be rewritten as Equation (15) by using the definition of Equation (16):

$$\phi_{g,j}^{coarse(n)} - \phi_{g,j}^{fine(n)} = \frac{\Sigma_{t,g,j}^{(m)}}{\Sigma_{t,g,j}^{(n)}} F_{g,j}^{(m)}$$
$$+ \frac{1}{\Sigma_{t,g,j}^{(n)} V_j} \sum_i \left(P_{g,ij}^{coarse(n)} - P_{g,ij}^{fine(n)} \right) \left(Q_{g,i}^{(n)} - Q_{g,i}^{(m)} \right) V_i \quad , \quad (15)$$
$$+ \frac{1}{\Sigma_{t,g,j}^{(n)} V_j} \sum_i \left\{ \left(P_{g,ij}^{coarse(n)} - P_{g,ij}^{fine(n)} \right) - \left(P_{g,ij}^{coarse(m)} - P_{g,ij}^{fine(m)} \right) \right\} Q_{g,i}^{(m)} V_i$$

$$F_{g,j}^{(m)} \equiv \phi_{g,j}^{coarse(m)} - \phi_{g,j}^{fine(m)} = \frac{1}{\Sigma_{t,g,j}^{(m)} V_j} \sum_i \left(P_{g,ij}^{coarse(m)} - P_{g,ij}^{fine(m)} \right) Q_{g,i}^{(m)} V_i \,, \quad (16)$$

where

$F_{g,j}^{(m)}$: difference of fine and coarse neutron fluxes evaluated at *m*-th burnup step, *g*-th energy group and *j*-th region.

The first term of the right hand side of Equation (15) is composed of $F_{g,j}^{(m)}$, which represents a difference of fine and coarse neutron fluxes at *m*-th burnup step, and a ratio of total cross sections. This term can be interpreted as an approximated difference of neutron flux at *n*-th burnup step projected with that of *m*-th burnup step, if each neutron flux is assumed to be inversely proportional to total cross section. Therefore, a corrected neutron flux newly proposed as Equation (17) is expected be closer to the fine neutron flux compared to the original coarse neutron flux:

$$\phi_{g,j}^{corrected[m](n)} = \phi_{g,j}^{coarse(n)} - \frac{\Sigma_{t,g,j}^{(m)}}{\Sigma_{t,g,j}^{(n)}} F_{g,j}^{(m)}, \tag{17}$$

where

$\phi_{g,j}^{corrected[m],(n)}$: neutron flux of *n*-th burnup step, *g*-th energy group and *j*-th region corrected by the difference of fine and coarse neutron fluxes evaluated at *m*-th burnup step.

By using the corrected neutron flux shown in Equation (17), Equation (18) can be derived from Equation (15):

$$\begin{aligned}\phi_{g,j}^{corrected[m](n)} - \phi_{g,j}^{fine(n)} = & \frac{1}{\Sigma_{t,g,j}^{(n)} V_j} \sum_i \left(P_{g,ij}^{coarse(n)} - P_{g,ij}^{fine(n)}\right)\left(Q_{g,i}^{(n)} - Q_{g,i}^{(m)}\right) V_i \\ & + \frac{1}{\Sigma_{t,g,j}^{(n)} V_j} \sum_i \left\{\left(P_{g,ij}^{coarse(n)} - P_{g,ij}^{fine(n)}\right) - \left(P_{g,ij}^{coarse(m)} - P_{g,ij}^{fine(m)}\right)\right\} Q_{g,i}^{(m)} V_i\end{aligned} . \tag{18}$$

Two terms in the right hand side of Equation (18) correspond to the discretization errors when the corrected neutron fluxes shown in Equation (17) is applied. The corrected neutron fluxes are based on the differences of fine and coarse neutron fluxes evaluated at *m*-th burnup step. Therefore, the corrected neutron fluxes can be easily evaluated when fixed source calculations with fine and coarse conditions are performed at *m*-th burnup step as similar to the calculation scheme of the SPH method. In this correction, the first term of the right hand side of Equation (15) is simply subtracted from the original coarse neutron flux. Now we remind that an approximation (i.e., neutron flux is inversely proportional to the total cross section) is used to derive Equation (17). Thus, accuracy of this correction would be improved by adjusting the magnitude of correction term, i.e., the second term of the right hand side of Equation (17). From this idea, a spatially independent scaling factor is introduced to improve the correction as shown in Equation (19):

$$\hat{\phi}_{g,j}^{corrected[m](n)} = \phi_{g,j}^{coarse(n)} - \lambda_g^{(n)} \frac{\Sigma_{t,g,j}^{(m)}}{\Sigma_{t,g,j}^{(n)}} F_{g,j}^{(m)}, \tag{19}$$

where

$\lambda_g^{(n)}$: scaling factor for $F_{g,j}^{(m)}$ of *n*-th burnup step and *g*-th energy group (spatially independent parameter),

$\hat{\phi}_{g,j}^{corrected[m],(n)}$: neutron flux of *n*-th burnup step, *g*-th energy group and *j*-th region corrected by the scaling factor and the difference of fine and coarse neutron fluxes evaluated at *m*-th burnup step.

By using the corrected flux shown in Equation (19), Equation (15) can be transformed into Equation (20):

$$\begin{aligned}\hat{\phi}_{g,j}^{corrected[m](n)} - \phi_{g,j}^{fine(n)} = &\left(1-\lambda_g^{(n)}\right)\frac{\Sigma_{t,g,j}^{(m)}}{\Sigma_{t,g,j}^{(n)}}F_{g,j}^{(m)} \\ &+\frac{1}{\Sigma_{t,g,j}^{(n)}V_j}\sum_i\left(P_{g,ij}^{coarse(n)}-P_{g,ij}^{fine(n)}\right)\left(Q_{g,i}^{(n)}-Q_{g,i}^{(m)}\right)V_i \\ &+\frac{1}{\Sigma_{t,g,j}^{(n)}V_j}\sum_i\left\{\left(P_{g,ij}^{coarse(n)}-P_{g,ij}^{fine(n)}\right)-\left(P_{g,ij}^{coarse(m)}-P_{g,ij}^{fine(m)}\right)\right\}Q_{g,i}^{(m)}V_i\end{aligned} \quad . \quad (20)$$

By substituting Equation (16) to Equation (20) and using Equation (12), Equation (21) is derived:

$$\begin{aligned}\hat{\phi}_{g,j}^{corrected[m](n)} - \phi_{g,j}^{fine(n)} = &\frac{1}{\Sigma_{t,g,j}^{(n)}V_j}\sum_i\left(P_{g,ij}^{coarse(n)}-P_{g,ij}^{fine(n)}\right)\left(Q_{g,i}^{(n)}-\lambda_g^{(n)}Q_{g,i}^{(m)}\right)V_i \\ &+\frac{\lambda_g^{(n)}}{\Sigma_{t,g,j}^{(n)}V_j}\sum_i\left(\Delta P_{g,ij}^{coarse(m,n)}-\Delta P_{g,ij}^{fine(m,n)}\right)Q_{g,i}^{(m)}V_i\end{aligned} \quad . \quad (21)$$

The right hand side of Equation (21) is similar to that of Equation (13), which is the equation for the SPH method. However, unlike the situation in the SPH method, the first term of the right hand side of Equation (21) could be reduced, since this term includes the scaling factor as additional freedom. As the next step of the derivation, determination of the scaling factor is discussed.

From the reciprocity theorem, Equation (22) is generally satisfied among collision probabilities, total cross sections and region volumes:

$$P_{g,ij}\Sigma_{t,g,i}V_i = P_{g,ji}\Sigma_{t,g,j}V_j \,. \tag{22}$$

By using the reciprocity theorem described in Equation (22), which is satisfied in each of coarse and fine conditions, and the definition of Equation (23), Equation (21) can be rewritten as Equation (24):

$$R_{g,i}^{(m,n)} \equiv \frac{Q_{g,i}^{(n)} - \lambda_g^{(n)} Q_{g,i}^{(m)}}{\Sigma_{t,g,i}^{(n)}}, \tag{23}$$

$$\begin{aligned}\hat{\phi}_{g,j}^{corrected[m](n)} - \phi_{g,j}^{fine(n)} = &\sum_i \left(P_{g,ji}^{coarse(n)} - P_{g,ji}^{fine(n)}\right) R_{g,i}^{(m,n)} \\ &+ \frac{\lambda_g^{(n)}}{\Sigma_{t,g,j}^{(n)} V_j} \sum_i \left(\Delta P_{g,ij}^{coarse(m,n)} - \Delta P_{g,ij}^{fine(m,n)}\right) Q_{g,i}^{(m)} V_i \end{aligned}. \tag{24}$$

The first term of the right hand side of Equation (24) becomes zero when R values are constant through all regions, since a summation of collision probabilities becomes unity. This fact indicates that spatial variance of Equation (23) have impact on the calculation error which comes from the first term of the right hand side of Equation (24). From this idea, in the present approach, the scaling factor is determined by minimizing a variance of Equation (23). The variance of Equation (23) is defined as Equation (25) by using the definition for the average shown in Equation (26):

$$VAR\left(R_g^{(m,n)}\right) \equiv \sum_i \omega_i \left\{ AVE\left(R_g^{(m,n)}\right) - \frac{Q_{g,i}^{(n)} - \lambda_g^{(n)} Q_{g,i}^{(m)}}{\Sigma_{t,g,i}^{(n)}} \right\}^2, \tag{25}$$

$$AVE\left(R_g^{(m,n)}\right) \equiv \sum_j \omega_j \frac{Q_{g,j}^{(n)} - \lambda_g^{(n)} Q_{g,j}^{(m)}}{\Sigma_{t,g,j}^{(n)}}, \tag{26}$$

where

ω_i : weighting factor of i-th region for evaluating the average and variance values.

In the present study, fraction of region volume is used as the weighting factor shown in Equations (25) and (26):

$$\omega_i = \frac{V_i}{\sum_j V_j}. \tag{27}$$

The variance described as Equation (25) is minimized when the derivative of the variance becomes zero. Therefore, the scaling factor which minimize the variance is obtained from the following equation:

$$\frac{\partial VAR\left(R_g^{(m,n)}\right)}{\partial \lambda_g^{(n)}} = 0. \tag{28}$$

Solving Equation (28), the scaling factor which minimizes the variance can be derived as Equation (29):

$$\lambda_g^{[m],(n)} = \frac{\left(\sum_i V_i\right)\left\{\sum_i V_i \left(\frac{Q_{g,i}^{(m)}}{\Sigma_{t,g,i}^{(n)}}\right)\left(\frac{Q_{g,i}^{(n)}}{\Sigma_{t,g,i}^{(n)}}\right)\right\} - \left(\sum_i V_i \frac{Q_{g,i}^{(m)}}{\Sigma_{t,g,i}^{(n)}}\right)\left(\sum_i V_i \frac{Q_{g,i}^{(n)}}{\Sigma_{t,g,i}^{(n)}}\right)}{\left(\sum_i V_i\right)\left\{\sum_i V_i \left(\frac{Q_{g,i}^{(m)}}{\Sigma_{t,g,i}^{(n)}}\right)^2\right\} - \left(\sum_i V_i \frac{Q_{g,i}^{(m)}}{\Sigma_{t,g,i}^{(n)}}\right)^2}. \tag{29}$$

It should be noted that suffix of '*m*' is added to the scaling factor in Equation (29) since it depends also on neutron sources of *m*-th burnup step. The present approach explained above and the scaling factor given by Equation (29) are referred to as the SVM (Source ratio Variance Minimization) method and the SVM factor, respectively. From Equations (16), (19) and (21), equations for the SVM method can be summarized as Equations (30) and (31):

$$\phi_{g,j}^{SVM[m],(n)} = \phi_{g,j}^{coarse(n)} - \lambda_g^{[m](n)} \frac{\Sigma_{t,g,j}^{(m)}}{\Sigma_{t,g,j}^{(n)}} \left(\phi_{g,j}^{coarse(m)} - \phi_{g,j}^{fine(m)}\right), \tag{30}$$

$$\phi_{g,j}^{SVM[m],(n)} - \phi_{g,j}^{fine(n)} = \frac{1}{\Sigma_{t,g,j}^{(n)} V_j} \sum_i \left(P_{g,ij}^{coarse(n)} - P_{g,ij}^{fine(n)} \right) \left(Q_{g,i}^{(n)} - \lambda_g^{(n)} Q_{g,i}^{(m)} \right) V_i + \frac{\lambda_g^{[m](n)}}{\Sigma_{t,g,j}^{(n)} V_j} \sum_i \left(\Delta P_{g,ij}^{coarse(m,n)} - \Delta P_{g,ij}^{fine(m,n)} \right) Q_{g,i}^{(m)} V_i \quad , \qquad (31)$$

where

$\phi_{g,j}^{SVM[m],(n)}$: neutron flux of *n*-th burnup step, *g*-th energy group and *j*-th region based on the difference of fine and coarse neutron fluxes evaluated at *m*-th burnup step.

In the right hand side of Equation (30), when the correction term (the second term) is larger than the original neutron flux (the first term), the corrected neutron flux becomes negative value. Thus, it should be noted that positivity of the corrected neutron flux is not guaranteed. However, we have never experienced the numerical instability caused by negative neutron fluxes in test calculations including the verifications described in Section 3.

From a comparison between Equations (5) and (31), it can be confirmed that the equation for the discretization errors in the SVM method becomes identical with that in the convention MOC when the all SVM factors are zero. On the other hand, from a comparison between Equations (13) and (31), the equation in the SVM method becomes the same form with that in the SPH method when the all SVM factors are unity. Although both of two terms in the right hand side of Equation (31) are the terms for the discretization errors, the first term is expected to be small since this term is minimized by using the SVM factors. Therefore, the calculation error would be dominated by the second term. In such case, a criterion for an update of the difference of neutron fluxes for the SVM method, which is shown in Equation (16), can be easily determined because the discretization errors mainly depend on changes of total cross sections.

As another topic, a necessity of a normalization of neutron fluxes should be discussed when a correction method on neutron fluxes is applied. If a summation of reaction rates through all regions is changed by a correction, neutron fluxes have to be normalized to

preserve neutron balance. In the case of the SVM method, the summation of the reaction rates can be written as Equation (32):

$$\sum_j \Sigma_{t,g,j}^{(n)} \phi_{g,j}^{SVM[m],(n)} V_j = \sum_j \Sigma_{t,g,j}^{(n)} \phi_{g,j}^{coarse(n)} V_j - \lambda_g^{[m](n)} \sum_j \Sigma_{t,g,j}^{(m)} \left(\phi_{g,j}^{coarse(m)} - \phi_{g,j}^{fine(m)} \right) V_j . \quad (32)$$

Equation (32) can be transformed into Equation (33) by using collision probabilities:

$$\sum_j \Sigma_{t,g,j}^{(n)} \phi_{g,j}^{SVM[m],(n)} V_j = \sum_j \Sigma_{t,g,j}^{(n)} \phi_{g,j}^{coarse(n)} V_j - \lambda_g^{[m](n)} \sum_i Q_i V_i \sum_j \left(P_{g,ij}^{coarse(m)} - P_{g,ij}^{fine(m)} \right). \quad (33)$$

The second term of the right hand side of Equation (33) can be eliminated, because a summation of collision probabilities becomes unity. Therefore, Equation (34) is derived as the equation for the summation of reaction rates:

$$\sum_j \Sigma_{t,g,j}^{(n)} \phi_{g,j}^{SVM[m],(n)} V_j = \sum_j \Sigma_{t,g,j}^{(n)} \phi_{g,j}^{coarse(n)} V_j . \quad (34)$$

Equation (34) indicates that the normalization of neutron fluxes is not necessary since neutron balance is preserved through the SVM method.

From the above discussions, the calculation procedure of the SVM method is described as follows:

(Steps 1 to 4 are performed at the burnup step where the update is carried out)

Step 1: Neutron sources for the following fixed source calculations are evaluated by one transport sweep with a coarse condition. (the same manner with the calculation scheme of the SPH method)

Step 2: Fixed source calculation with a fine condition is carried out.

Step 3: Fixed source calculation with a coarse condition is carried out.

Step 4: The difference of neutron fluxes shown in Equation (16) are evaluated.

(Steps 5 and 6 are performed at all burnup steps)

Step 5: The SVM factors are evaluated by Equation (29) after fission and scattering sources are updated during inner iteration.

Step 6: Neutron fluxes are corrected by Equation (30) after each inner iteration.

As the same procedure with the SPH method, in the present study, fixed source calculations are performed instead of eigenvalue calculations at Steps 2 and 3 in order to reduce additional calculation time for the SVM method. The detail of the calculation procedure of the SVM method can be shown in **Figure 2**.

< Figure 2 >

In section 2, equations for the discretization errors are derived as Equations (5), (13) and (31) for the conventional MOC, the SPH method and the SVM method, respectively. Calculation accuracy of each method is tested through some verification calculations described in the next section.

3. Verifications

3.1. Verifications in single assembly geometries

In order to confirm accuracy of the SPH and SVM methods, verification calculations are performed in PWR single assembly geometries by the AEGIS code [13]. Four types of calculation cases named ‘ORG’, ‘SPH’, ‘SVM’ and ‘SVM_UD’ listed below are assumed in this verification and those results are compared to the reference result.

- ORG: depletion calculations are performed with the conventional MOC.

- SPH: depletion calculations are performed with the SPH method (the SPH factors are evaluated at the first burnup step and not updated).
- SVM: depletion calculations are performed with the SVM method (the differences of neutron fluxes between fine and coarse calculation conditions are evaluated at the first step and not updated).
- SVM_UD: depletion calculations are performed with the SVM method (the difference of neutron fluxes are updated when the maximum change of total cross sections in flat flux regions exceeds 20%).

In order to evaluate the basic capabilities of the SPH and SVM methods, the SPH factors and the differences of neutron fluxes for the SVM method are not updated during depletion calculations in the SPH and SVM cases. On the other hand, in the SVM_UD case, the differences of neutron fluxes are updated according to the change of total cross sections in order to investigate an impact of the update. The change of total cross sections in the definition of SVM_UD means a change from the total cross sections at the latest updated step. In order to minimize the additional calculation time for the update, the differences of neutron fluxes are updated only in the energy group whose change of total cross section is significant. Although an update of the SPH factors can be done by a similar manner, a criteria for updating the SPH factors is difficult to determine because the discretization errors depend on changes of two parameters as mentioned in the previous section. Therefore, update of the SPH factors is not carried out in this test. The calculation geometries are listed below and illustrated in **Figure 3**. These geometries are chosen as representatives of PWR single assembly.

- 4.8 wt% UO_2 fuel (‘UO2’)
- 4.8 wt% UO_2 fuel with control rods insertion (‘RCC’)
- 10.0 wt% Gd bearing 4.8 wt% fuel (‘GAD’)

- 4.0, 8.0, 12.0 wt% Pu-total MOX fuel (‘MOX’)

< Figure 3 >

In this paper, the above calculation geometries are called as UO2, RCC, GAD and MOX, respectively. The ray tracing and calculation conditions are listed in **Tables 1** and **2**. As shown in Table 1, two types of ray tracing conditions, i.e. the fine and coarse conditions, are used. In ORG, SPH and SVM cases, the coarse condition shown in Table 1 is used for the calculations. The reference results are obtained by the conventional MOC calculations with the fine condition shown in Table 1.

< Table 1 >

< Table 2 >

In all cases of the calculations, differences of k-infinity and pin wise fission rate from those of the reference results are evaluated. The results of the k-infinity differences are shown in **Figure 4**, and those of the maximum pin wise fission rate differences are shown in **Figure 5**. Additionally, the maximum differences through depletion calculations are summarized in **Table 3**.

< Figure 4 >

< Figure 5 >

< Table 3 >

From the results of the SPH case, it is confirmed that differences from the reference results are not improved in some cases in Table 3. Especially, in Gd bearing fuel assembly, differences become extremely large in the SPH method as expected since neutron sources and total cross sections are drastically changing through the depletion in such geometry. From these results, the SPH method in the present scheme is not suitable for depletion calculations.

In the SVM case, differences from the reference results are smaller than those in the conventional MOC in most of the cases in Table 3 except for pin wise fission rate difference in Gd bearing fuel assembly. On the other hand, in the SVM_UD case, differences from the reference results are decreased in all items in Table 3. These results mean that the differences of neutron fluxes for the SVM method, which is shown in Equation (16), need to be updated according to changes of total cross sections to obtain accurate results. The differences in the SVM_UD case are stably small through depletion calculations and the maximum difference of k-infinity is approximately 0.05% and that of pin wise fission rate is smaller than 0.4%. These results are significantly better than those of the ORG case, i.e. 1.69% and 1.8% respectively. However, this comparison is not fair because there is the additional calculation time for the SVM method in the SVM_UD case. Therefore, relationships between accuracy and calculation time in each case are evaluated through calculations with five types of coarse ray tracing conditions listed in **Table 4**. In this table, the ray tracing conditions become finer as it goes downwards. The calculation time evaluated in this test includes time for transport sweep and the additional time for the SVM method (calculation time for other processes such as resonance calculations and burnup calculations are excluded from the calculation time). The results for k-infinity and the maximum pin wise fission rate differences are shown in **Figures 6** and **7**, respectively. In these figures, the horizontal axes are normalized so that calculation time with the coarsest condition, i.e. the coase_1 condition, becomes unity in each geometry.

< Table 4 >

< Figure 6 >

< Figure 7 >

Although the additional calculation time for the SVM method is approximately 20% at maximum, the differences in the SVM_UD case are significantly smaller than those in the

ORG case. Figures 6 and 7 indicate that the SVM method with the update gives enough accurate results by shorter calculation time compared to the conventional MOC. In the SVM_UD case with the coarse_3 condition, the maximum differences of k-infinity and pin wise fission rate are 0.01% and 0.1% respectively. In order to obtain the comparable accuracy in the ORG case, the coarse_5 condition is necessary. Comparing to the calculation time of these cases, the calculation time in the SVM_UD case is smaller than one third of that in the ORG case. From these results, improvement of calculation efficiency by the present approach is confirmed.

3.2. Multi Assembly Calculations

In order to test the present method in a geometry where a large spatial change of neutron flux appears, verification calculations are performed in PWR multi assembly geometry by the AEGIS code. In this verification, the 'ORG' and 'SVM_UD' cases defined above are assumed and those results are compared to the reference result. The calculation geometry is illustrated in **Figure 8**.

< Figure 8 >

The ray tracing and calculation conditions are the same with those of the verification in single assembly calculations (shown in Tables 1 and 2). The reference results are obtained by the conventional MOC calculations with the fine condition shown in Table 1. In all cases of the calculations, differences of k-infinity and pin wise fission rate from those of the reference results are evaluated. The results of the k-infinity differences are shown in **Figure 9**, and those of the maximum pin wise fission rate differences are shown in **Figure 10**. Additionally, the maximum differences through depletion calculations are summarized in **Table 5**.

< Figure 9 >

< Figure 10 >

< Table 5 >

The differences in the SVM_UD case are stably small through depletion calculations as similar to the results of single assembly calculations. The maximum difference of k-infinity is approximately 0.12% and that of pin wise fission rate is smaller than 0.4%. These results are significantly better than those of the ORG case, i.e. 1.15% and 3.6% respectively. However, as mentioned above, this comparison is not fair because there is the additional calculation time for the SVM method only in the SVM_UD case. Therefore, relationships between accuracy and calculation time in each case are evaluated through calculations with five types of coarse ray tracing calculations listed in Table 5. The definition of the calculation time is same with that in the single calculations (only calculation time for transport sweep and the addition calculation time for the SVM method). The results for k-infinity and the maximum pin wise fission rate differences are shown in **Figures 11** and **12**, respectively. In these figures, the horizontal axes are normalized so that calculation time with the coarsest condition becomes unity.

< Figure 11 >

< Figure 12 >

As similar to the results of the single assembly calculations, the differences can be significantly reduced by the SVM method with the update. In the SVM_UD case with the coarse_3 condition, the maximum differences of k-infinity and pin wise fission rate are 0.02% and 0.2% respectively. In order to obtain the comparable accuracy in the ORG case, the coarse_5 condition is necessary. Comparing to the calculation time of these cases, the calculation time in the SVM_UD case is smaller than quarter of that in the ORG case. From these results, improvement of calculation efficiency by the present approach is confirmed

including in the geometry where large spatial change of neutron flux appears.

4. Conclusions

In this paper, efficient calculation schemes for MOC to reduce discretization errors of ray tracing are investigated focusing on depletion calculations. As the first step of the present study, a calculation scheme using the SPH method is considered. As results of derivations, it is found that the discretization errors in this scheme are caused by changes of neutron sources and total cross sections according to a depletion. From this fact, in this study, a new approach is proposed to mitigate the problem of the SPH method. In the new approach called the SVM method, the discretization error caused by changes of neutron sources can be reduced by minimizing a variance of a certain parameter which is composed of a ratio of neutron source to total cross section.

The verification calculations are performed in PWR single and multi assembly geometries to evaluate accuracy and calculation efficiency of the SPH and SVM methods. The verification results indicate that differences from the reference results are degraded in some cases in the SPH method. Especially in a calculation of Gd bearing fuel assembly, the differences by the SPH method becomes extremely larger than those by the conventional MOC. On the other hand, the SVM method gives more accurate results compared to the conventional MOC in all calculations when a parameter related to the SVM method is updated according to changes of total cross sections. Although the update of the parameter in the SVM method needs additional calculation time, the results of accuracy and calculation time suggest that calculation efficiency can be improved by the SVM method in both of single and multi assembly calculations. Calculation time in the SVM method in single and multi assembly calculations are smaller than one third and quarter of that in the conventional MOC respectively to obtain comparable accuracy.

References

[1] Askew JR. A characteristics formulation of the neutron transport equation in complicated geometries. Winfrith: Atomic Energy Authority; 1972. (AEEW-M1108).

[2] Sugimura N, Yamamoto A, Ushio T, Mori M, Tabuchi M, Endo T. Neutron transport models of AEGIS: an advanced next-generation neutronics design system. Nucl. Sci. Eng. 2007; 155:276-289.

[3] Ushio T, Takeda T, Mori M. Neutron anisotropic scattering effect in heterogeneous cell calculations of light water reactors. J. Nucl. Sci. Technol. 2003 Jul; 40:464-480.

[4] Leonard A, McDaniel CT. Optimal polar angles and weights. Trans. Am. Nucl. Soc. 1995; 73:171.

[5] Yamamoto A, Tabuchi M, Sugimura N, Ushio T, Mori M. Derivation of optimum polar angle quadrature set for the method of characteristics based on approximation error for the Bickley function. J. Nucl. Sci. Technol. 2007 Feb; 44:129-136.

[6] Tabuchi M, Yamamoto A, Endo T, Sugimura N. Preservation of transmission probabilities in the method of characteristics. J. Nucl. Sci. Technol. 2013 May; 50:837-843.

[7] Kavenoky A. The SPH homogenization method. Proc. Meeting Homogenization Methods in Reactor Physics; 1978 Nov 13-15; Lugano. Lugano: IAEA-TECDOC-231, International Atomic Energy Agency; 1978.

[8] Giho A, Yoshida E, Miyawaki K, Ohori K, Umebara Y, Takeda T. Study on cross section corrections using SPH method for a whole core heterogeneous MOC calculation. Proc. PHYSOR-2014; 2014 Sep 28-Oct 3; Kyoto (Japan). [CD-ROM].

[9] Sugimura N, Yamamoto Akio. Resonance treatment based on ultra-fine group spectrum calculation in the AEGIS code. J. Nucl. Sci. Technol. 2007 Jul; 44:958-966.

[10] Tatsumi M, Yamamoto A. Advanced PWR core calculation based on multi-group nodal-transport method in three-dimensional pin-by-pin geometry. J. Nucl. Sci. Technol. 2003 Jun; 40:376-387.

[11] Yamamoto A, Kitamura Y, Ushio T, Sugimura N. Convergence improvement of coarse mesh rebalance method for neutron transport calculations. J. Nucl. Sci. Technol. 2004 Aug; 41:781-789.

[12] Yamamoto A. Generalized coarse-mesh rebalance method for acceleration of neutron transport calculations. Nucl. Sci. Eng. 2005; 151:274-282.

[13] Yamamoto A, Endo T, Tabuchi M, Sugimura N, Ushio T, Mori M, Tatsumi M. AEGIS: an advanced lattice physics code for light water reactor analyses. Nucl. Eng. Technol. 2010 May; 42:500-519.

[14] Sartori E. Standard energy group structures of cross section libraries for reactor shielding, reactor cell and fusion neutronics applications: VITAMIN-J, ECCO-33, Gir-sur-Yvette: NEA Data Bank; 1990.

[15] Stamm'ler RJJ, Abbate MJ, Methods of steady-state reactor physics in nuclear design. London: Academic Press; 1983.

Figure captions

Figure 1. Concept of the application of the SPH method to depletion calculations.

Figure 2. Flow char for the calculation procedure of the SVM method.

Figure 3. Geometries for single assembly calculations.

Figure 4. Differences of k-infinity (single assembly calculations).

Figure 5. Maximum differences of pin wise fission rate (single assembly calculations).

Figure 6. Relationship between difference of k-infinity and calculation time (single assembly calculations).

Figure 7. Relationship between maximum difference of pin wise fission rate and calculation time (single assembly calculations).

Figure 8. A geometry for multi assembly calculations.

Figure 9. Difference of k-infinity (multi assembly calculations).

Figure 10. Maximum difference of pin wise fission rate (multi assembly calculations).

Figure 11. Relationship between difference of k-infinity and calculation time (multi assembly calculations).

Figure 12. Relationship between maximum difference of pin wise fission rate and calculation time (multi assembly calculations).

Table 1. Ray tracing conditions used in the verification calculations.

	Ray separation (*1) [cm]	Number of azimuthal angle division (*2)	Number of polar angle division (*3)
coarse	0.50	8	1
fine	0.05	128	3

(*1) Macroband method with transmission probability preservation through linear approximation (TPPL) [6] is used. Values in this table mean the maximum ray separation (in average, ray separations are narrower).

(*2) Uniformly divided angle is used. Values in this table mean number of divisions for 2π.

(*3) The Tabuchi and Yamamoto's optimum quadrature set (TY quadrature set) [5] is used. Values in this table mean number of divisions for $\pi/2$.

Table 2. Calculation conditions used in the verification calculations

Number of energy groups	172 (XMAS group structure [14])
Scattering order	P0 (transport correction [15])
Burnup step	UO2, RCC and MOX: 0, 0.1, 0.5, 1, every 1 from 1 to 60
[GWd/t]	GAD: 0, 0.1, 0.5, every 0.5 from 0.5 to 30, every 1 from 30 to 60

Table 3. Maximum differences through depletions (single assembly calculations).

Geometry	Calculation case	Difference of k-infinity [%]	Difference of pin-by-pin fission rate [%]	
			RMS difference	Maximum difference
UO2	ORG	0.756	0.23	0.55
	SPH	0.640	0.22	0.56
	SVM	0.225	0.06	0.14
	SVM_UD	0.046	0.03	0.09
RCC	ORG	1.369	0.64	1.52
	SPH	0.269	0.34	0.85
	SVM	0.064	0.08	0.21
	SVM_UD	0.031	0.08	0.23
GAD	ORG	0.802	0.56	1.79
	SPH	8.521	7.94	29.37
	SVM	0.311	1.14	4.71
	SVM_UD	0.051	0.15	0.38
MOX	ORG	1.688	0.37	1.04
	SPH	0.408	1.39	4.16
	SVM	0.138	0.11	0.24
	SVM_UD	0.051	0.05	0.10

Table 4. Ray tracing conditions used for the evaluation of calculation efficiency.

	Ray separation (*1) [cm]	Number of azimuthal angle division (*2)	Number of polar angle division (*3)
coarse_1	0.50	8	1
coarse_2	0.20	16	2
coarse_3	0.10	32	2
coarse_4	0.10	64	3
coarse_5	0.05	96	3
fine	0.05	128	3

(*1) Macroband method with TPPL is used. Values in this table mean the maximum ray separation (in average, ray separations are narrower).

(*2) Uniformly divided angle is used. Values in this table mean number of divisions for 2π.

(*3) The TY quadrature set is used. Values in this table mean number of divisions for $\pi/2$.

Table 5. Maximum differences through depletions (multi assembly calculations).

Calculation case	Difference of k-infinity [%]	Difference of pin-by-pin fission rate [%]	
		RMS difference	Maximum difference
ORG	1.145	1.69	3.58
SVM_UD	0.121	0.16	0.36

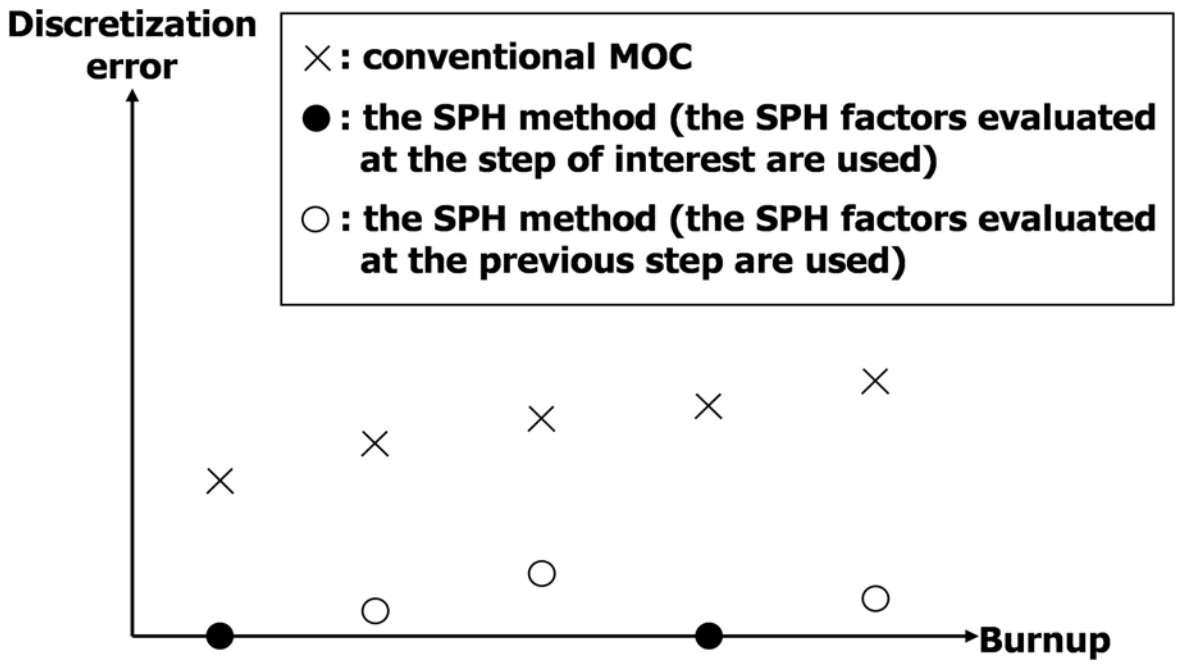

Figure 1. Concept of the application of the SPH method to depletion calculations.

M. Tabuchi:

Reduction of MOC discretization errors through a minimization of source ratio variances

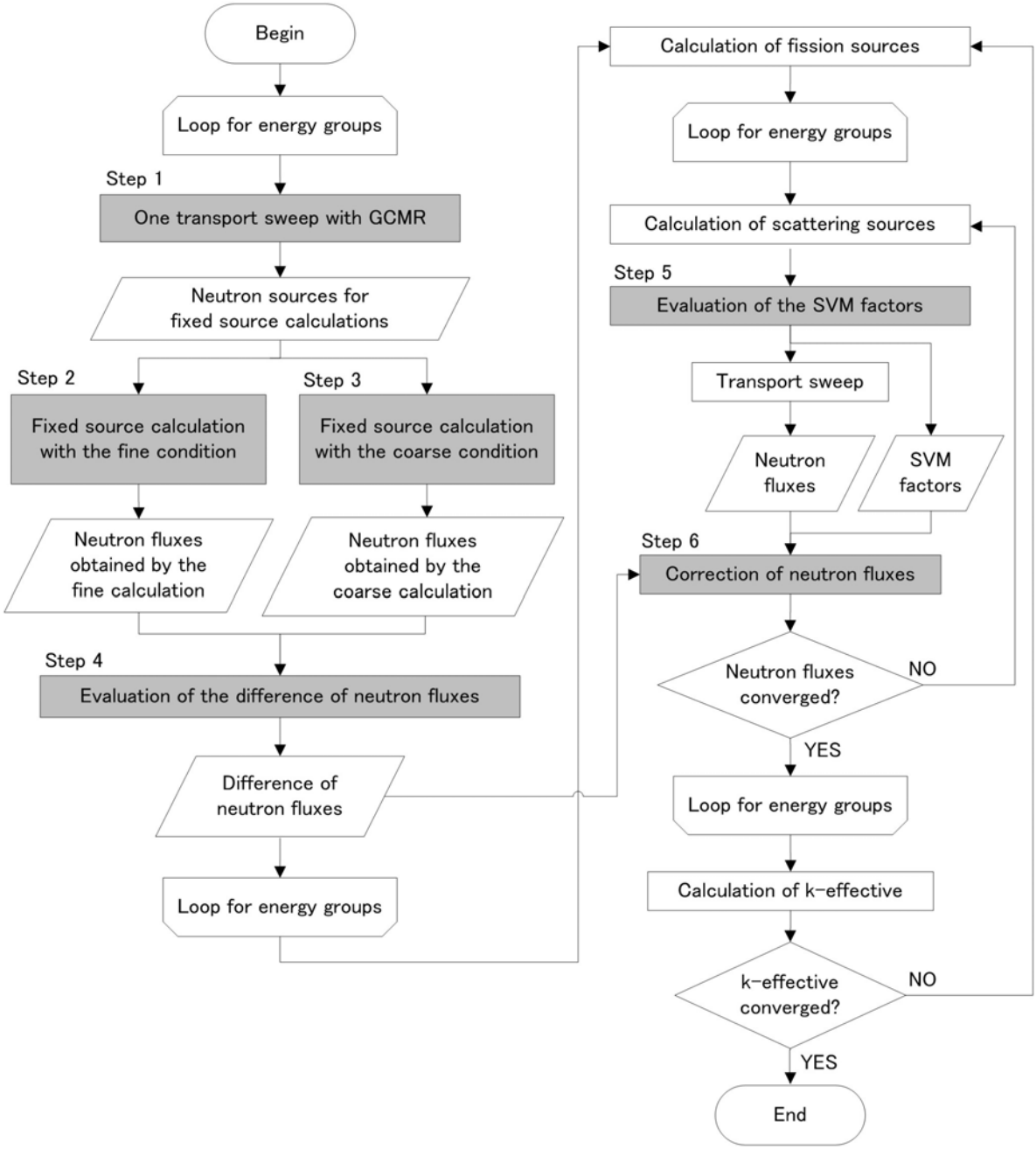

Figure 2. Flow chart for the calculation procedure of the SVM method.

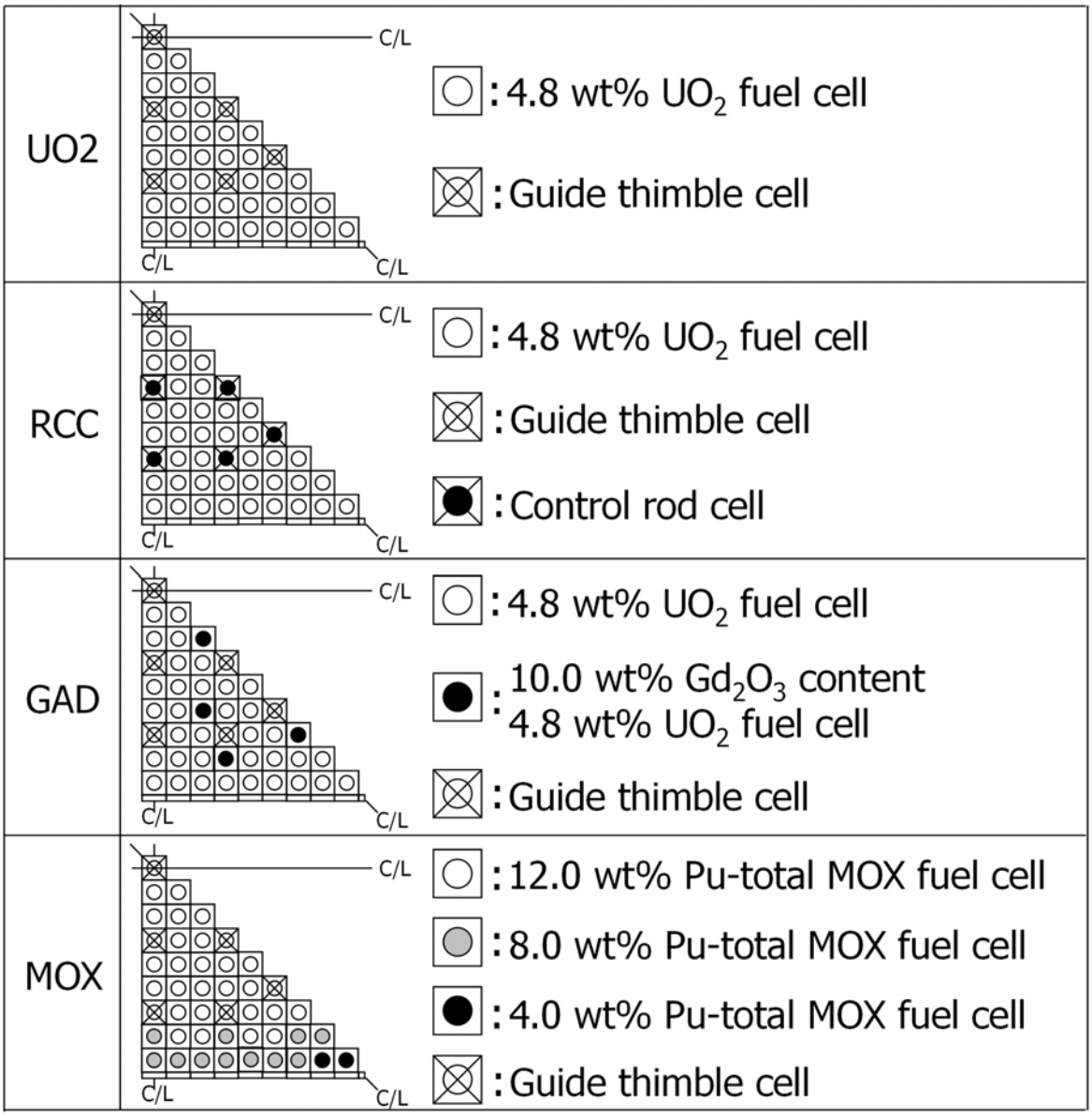

Figure 3. Geometries for single assembly calculations.

M. Tabuchi:

Reduction of MOC discretization errors through a minimization of source ratio variances

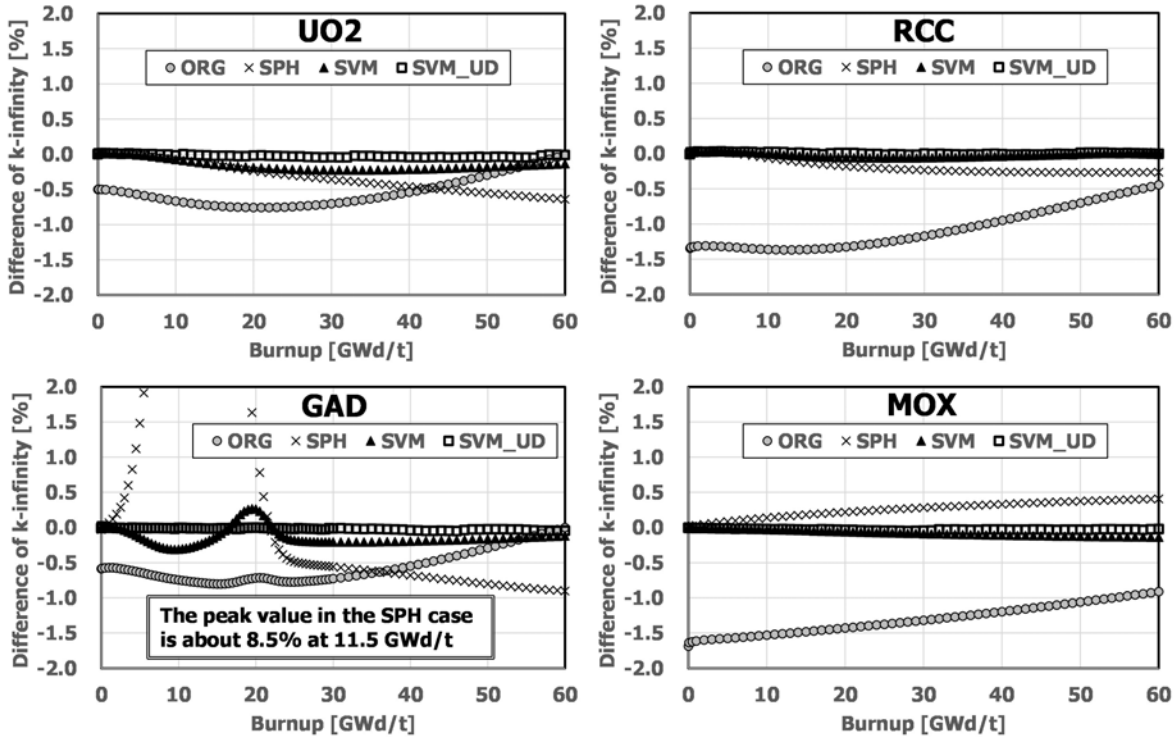

Figure 4. Differences of k-infinity (single assembly calculations).

M. Tabuchi:

Reduction of MOC discretization errors through a minimization of source ratio variances

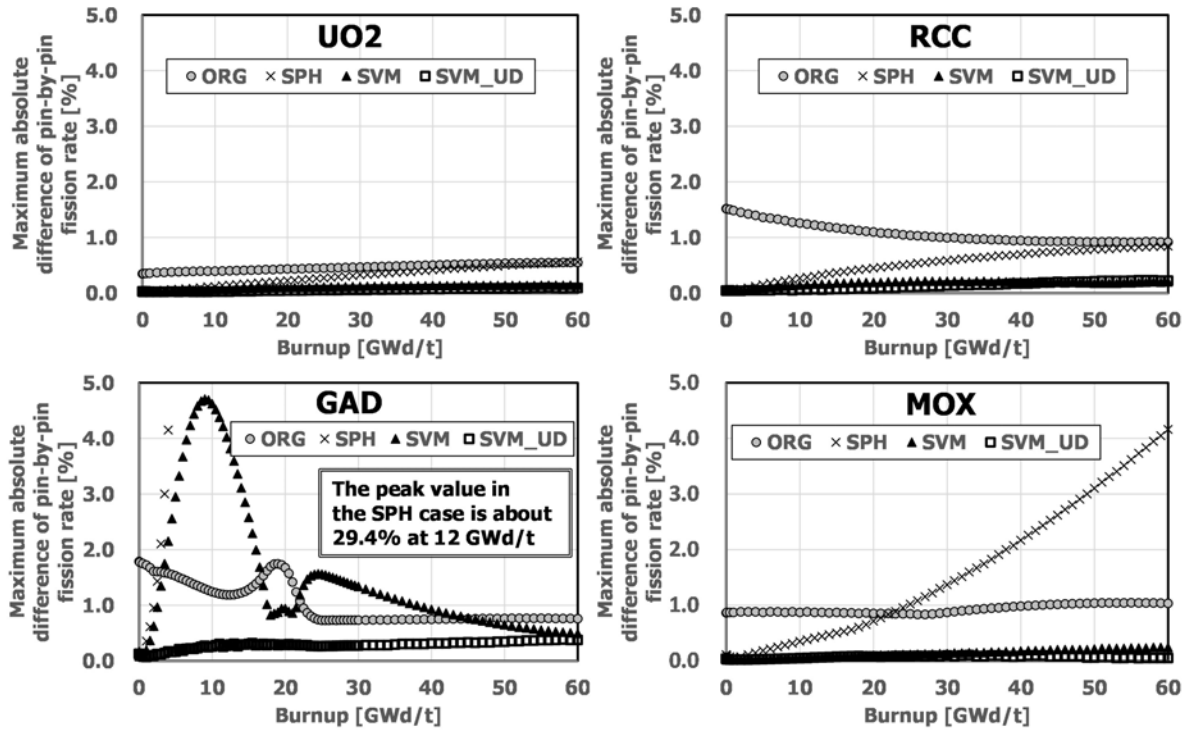

Figure 5. Maximum differences of pin wise fission rate (single assembly calculations).

M. Tabuchi:

Reduction of MOC discretization errors through a minimization of source ratio variances

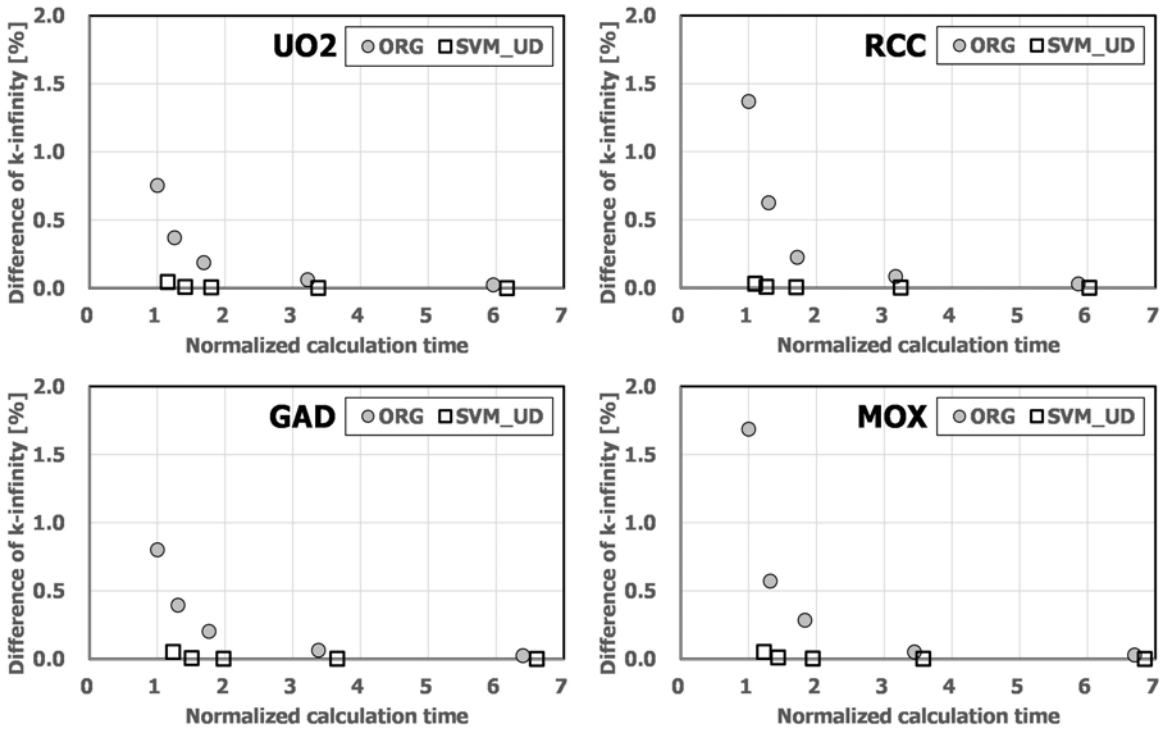

Figure 6. Relationship between difference of k-infinity and calculation time (single assembly calculations).

M. Tabuchi:

Reduction of MOC discretization errors through a minimization of source ratio variances

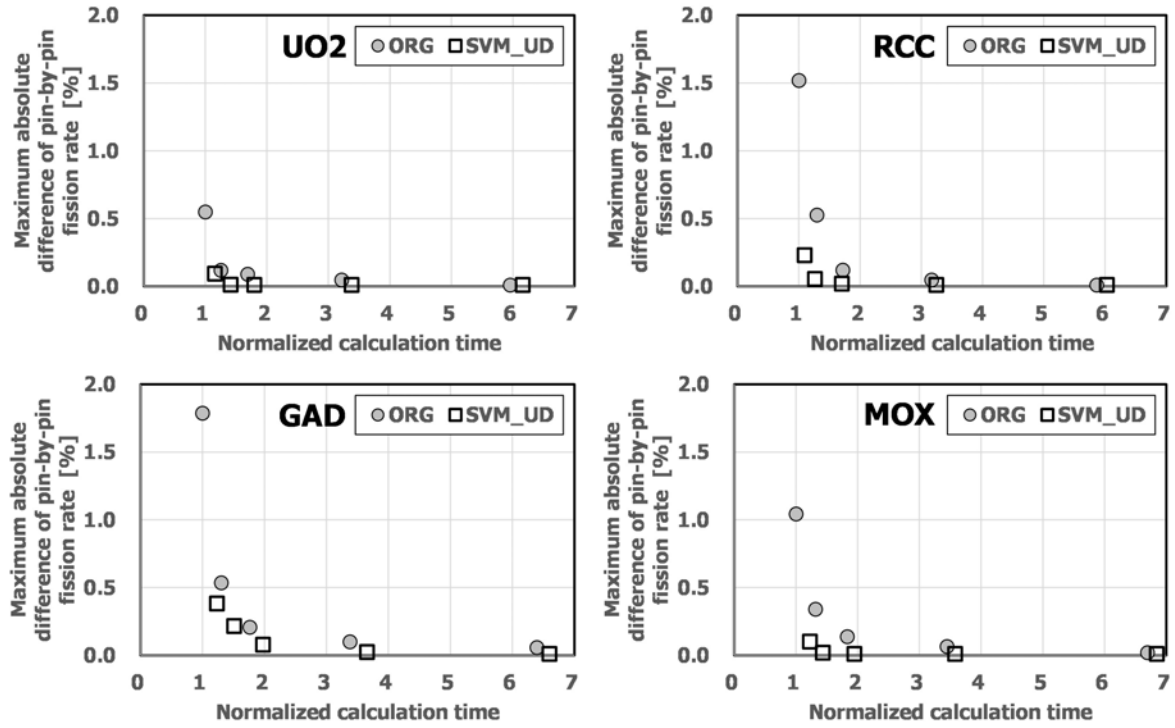

Figure 7. Relationship between maximum difference of pin wise fission rate and calculation time (single assembly calculations).

M. Tabuchi:

Reduction of MOC discretization errors through a minimization of source ratio variances

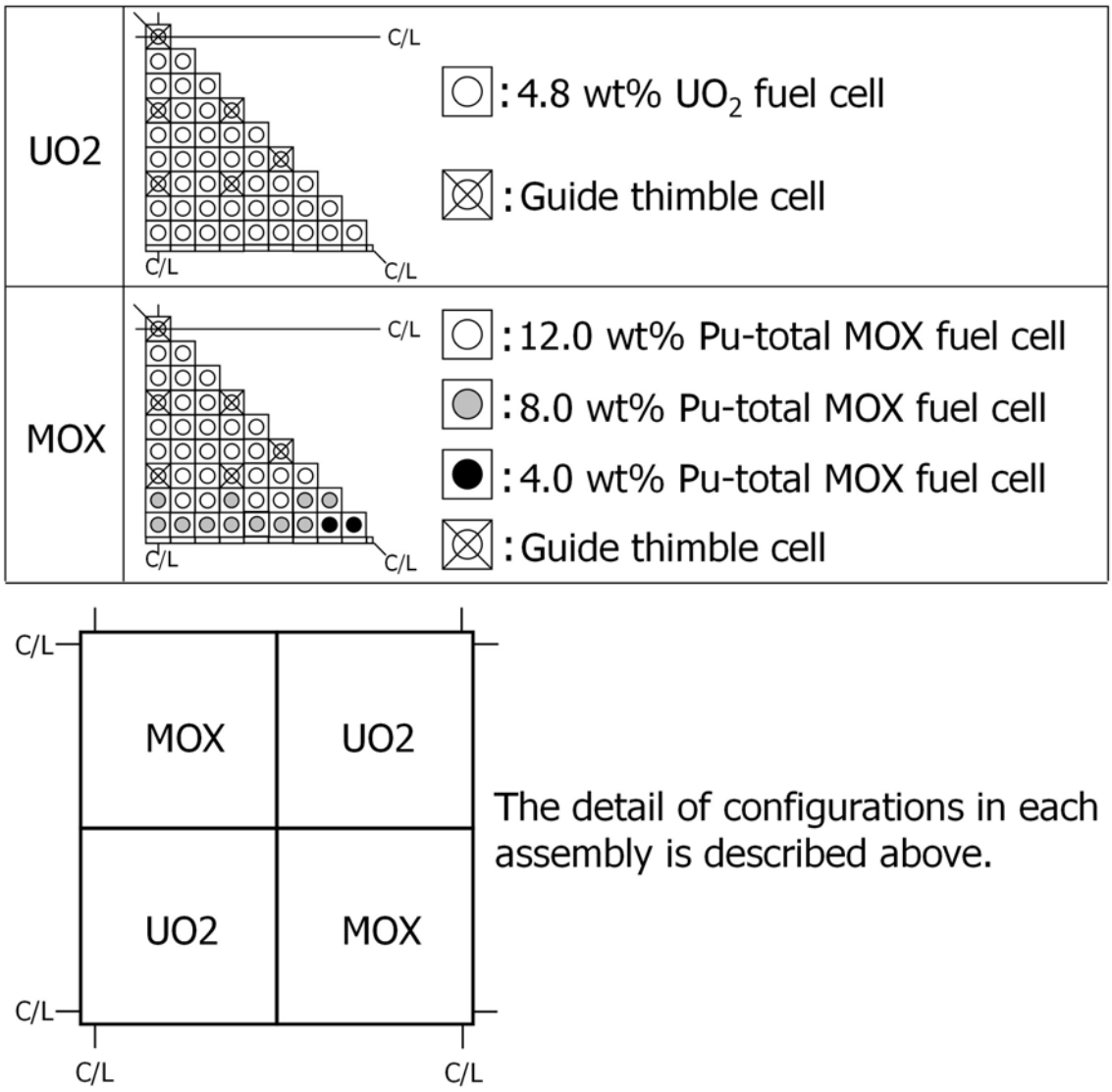

Figure 8. A geometry for multi assembly calculations.

M. Tabuchi:

Reduction of MOC discretization errors through a minimization of source ratio variances

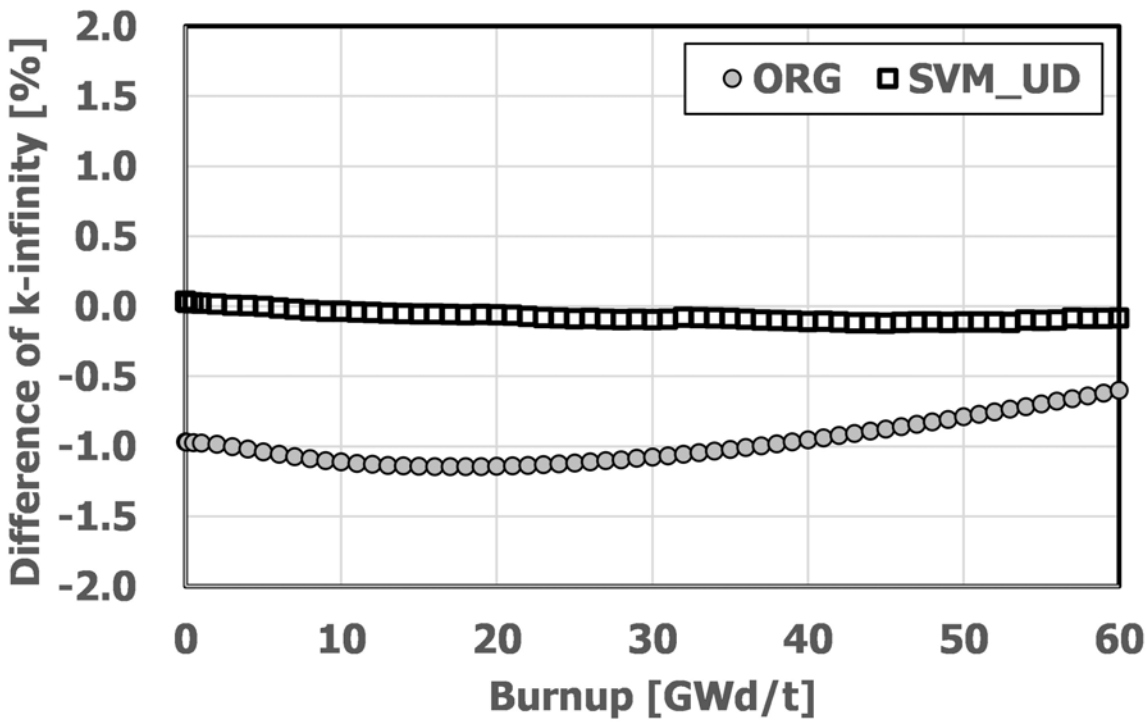

Figure 9. Difference of k-infinity (multi assembly calculations).

M. Tabuchi:

Reduction of MOC discretization errors through a minimization of source ratio variances

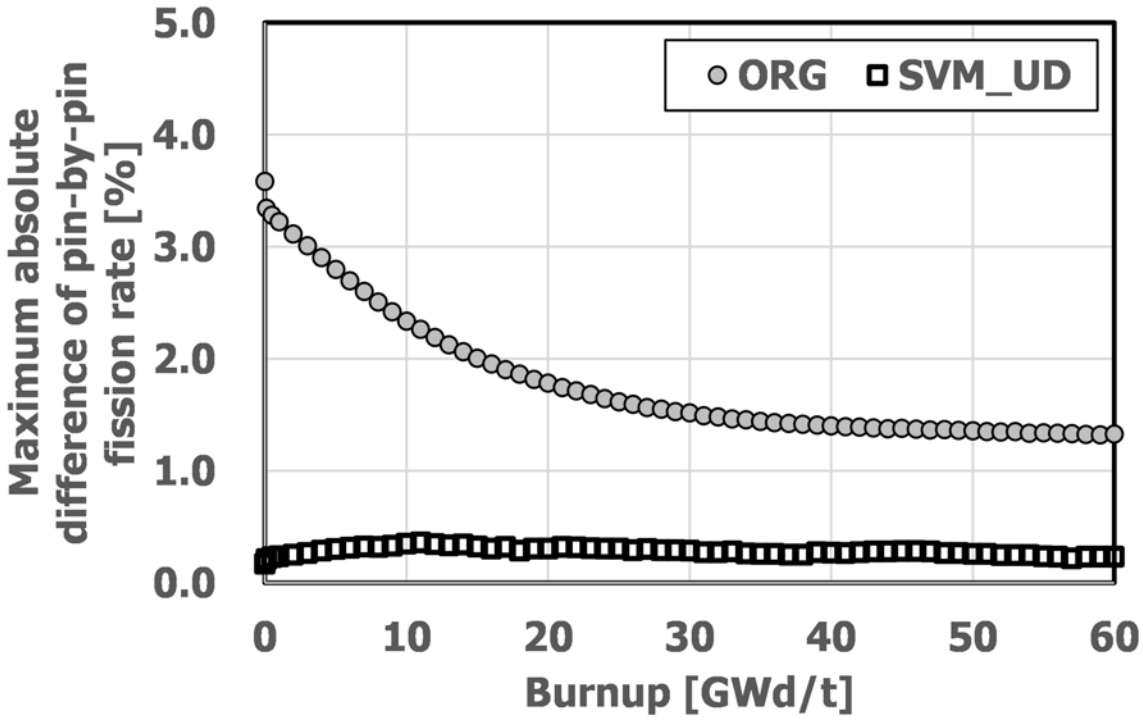

Figure 10. Maximum difference of pin wise fission rate (multi assembly calculations).

M. Tabuchi:

Reduction of MOC discretization errors through a minimization of source ratio variances

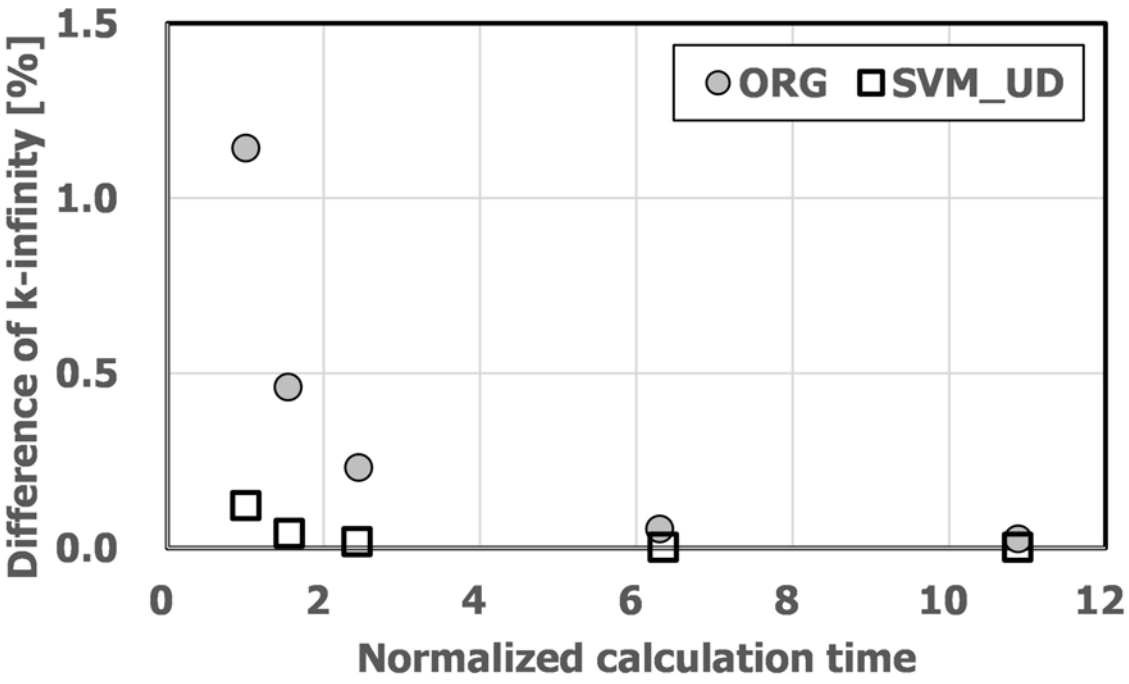

Figure 11. Relationship between difference of k-infinity and calculation time (multi assembly calculations).

M. Tabuchi:

Reduction of MOC discretization errors through a minimization of source ratio variances

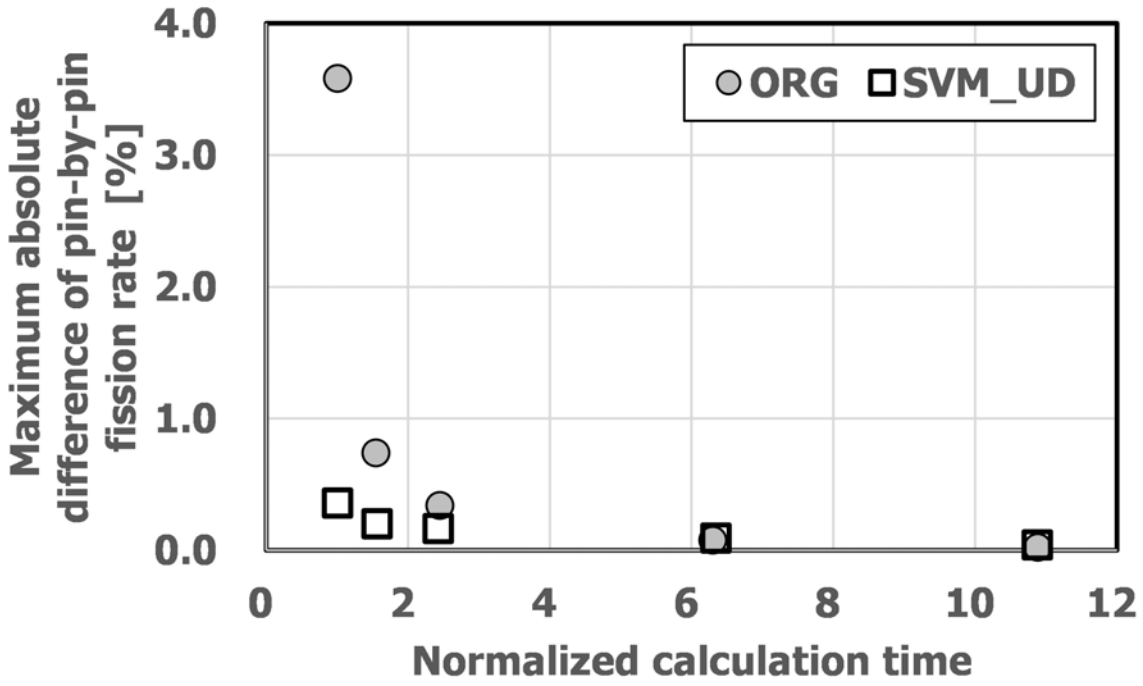

Figure 12. Relationship between maximum difference of pin wise fission rate and calculation time (multi assembly calculations).

M. Tabuchi:

Reduction of MOC discretization errors through a minimization of source ratio variances